Science Advances

AAAS

advances.sciencemag.org/cgi/content/full/4/1/eaao2623/DC1

Supplementary Materials for

Magnetosensitive e-skins with directional perception for augmented reality

Gilbert Santiago Cañón Bermúdez, Dmitriy D. Karnaushenko, Daniil Karnaushenko, Ana Lebanov, Lothar Bischoff, Martin Kaltenbrunner, Jürgen Fassbender, Oliver G. Schmidt, Denys Makarov

Published 19 January 2018, *Sci. Adv.* **4**, eaao2623 (2018)
DOI: 10.1126/sciadv.aao2623

The PDF file includes:

Other Supplementary Material for this manuscript includes the following:
(available at advances.sciencemag.org/cgi/content/full/4/1/eaao2623/DC1)

- movie S5 (.mp4 format). Demonstrator 2: Interactive light dimming by touchless manipulation.
- movie S6 (.mp4 format). Stability of the sensor response submerged in aqueous and saline solution.
- movie S7 (.mp4 format). Temperature stability of the novel ultrathin polyimide foils and a commercial foil.
- movie S8 (.mp4 format). Temperature compensation of the bridge.

Supplementary Materials

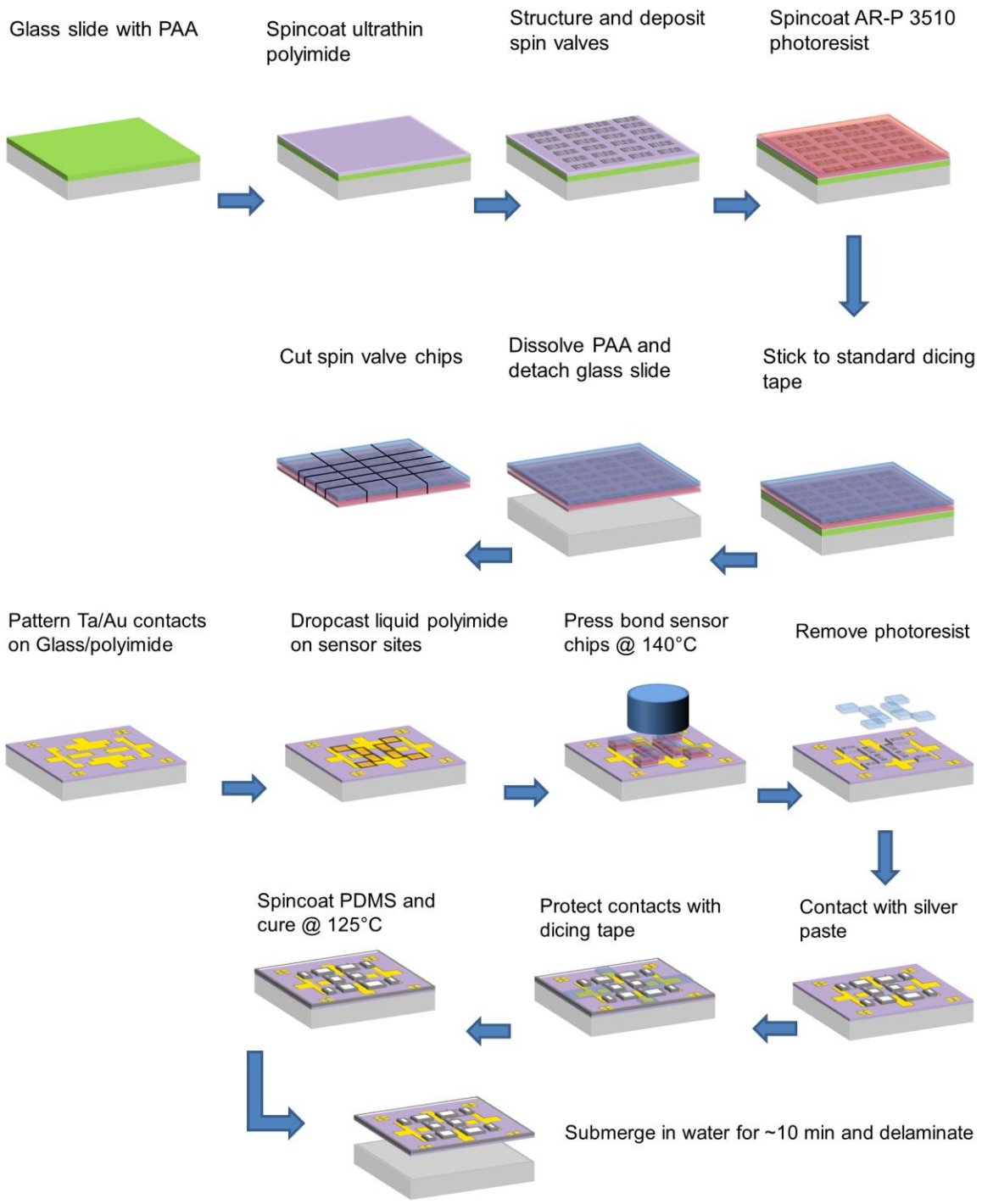

fig. S1. Fabrication flow. Schematics, summarizing the fabrication steps which were undertaken to prepare 2D magnetic field sensor on ultrathin polyimide foils.

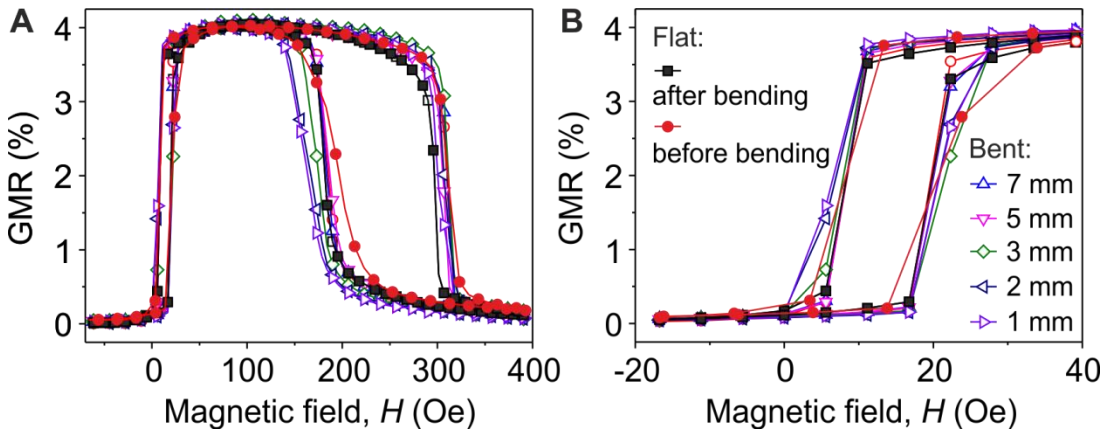

fig. S2. Mechanical characterization of spin valves. (**A**) GMR curves taken of a spin valve sensor element before bending, in a bent state down to a radius of curvature of 1 mm, and after bending. The close up of the hysteresis loops of the sensing layer is shown in (**B**). The legend in panel (B) is valid for panel (A) as well.

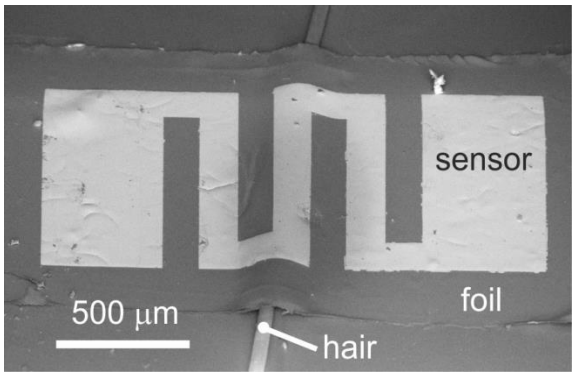

fig. S3. Compliancy of a flexible spin valve to a hair. SEM image of a spin valve sensor element located on and conforming to a hair.

fig. S4. Angle characterization setup. A permanent bar magnet is attached to the shaft of a stepper motor to provide a constant field in the plane of the 2D sensor. The sensor is fixed on a curved glass support suspended over the magnet such that the in-plane field magnitude is 50 Oe. Upon rotation of the magnet the angular response of the sensor is monitored at a computer.

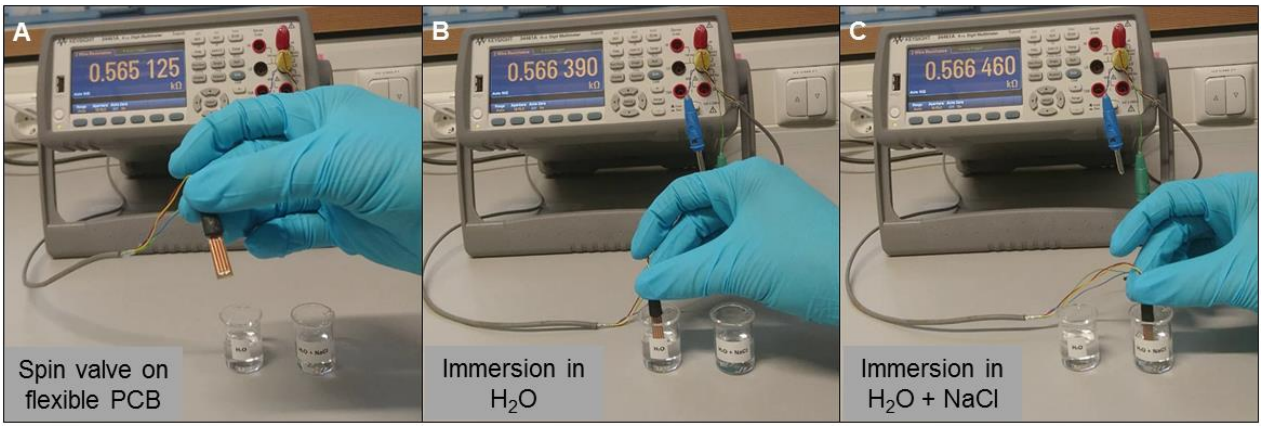

fig. S5. Encapsulation experiments for a spin valve sensor. Upon submerging a spin valve sensor on a flexible printed circuit board (PCB) (**A**) in DI water (**B**) and sweat-like saline solution of 40 mmol/L (**C**) the resistance of the device changes only slightly. In video S6, we demonstrate operation of the device when submerged for 30 s in DI water and in saline solution. We are currently investigating operational stability under such conditions for extended periods of time.

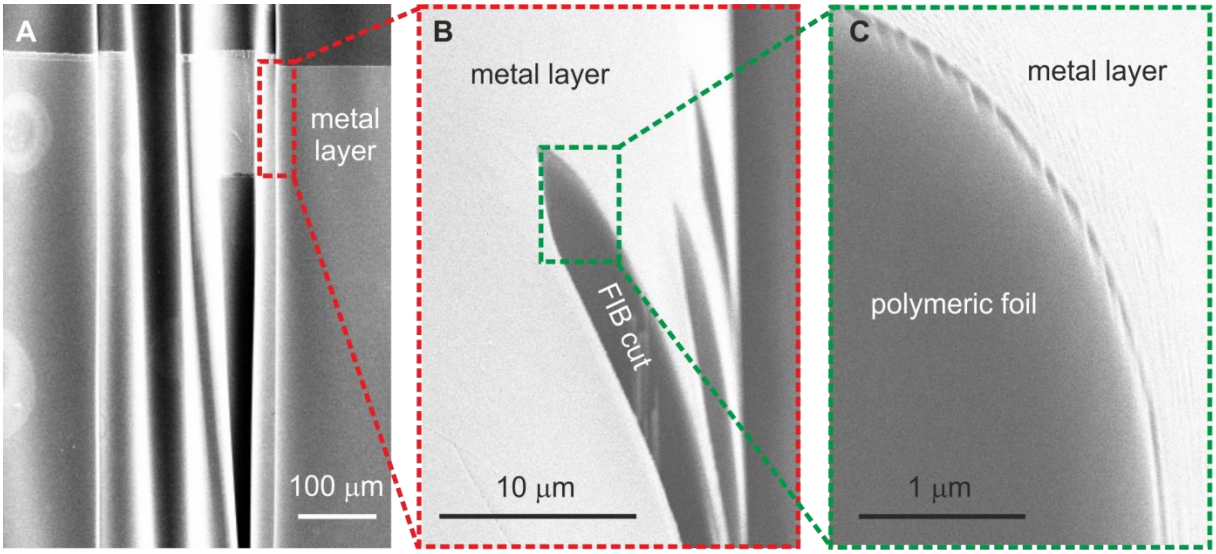

fig. S6. Mechanical stability of the sensor layer stack upon bending. (**A**) SEM top view image of a wrinkled spin valve sensor. The red frame shows the location of a FIB-cut region. The close up of this region is shown in (**B**). The zoom of the region indicated with a green frame in panel (**B**) is shown in (**C**).

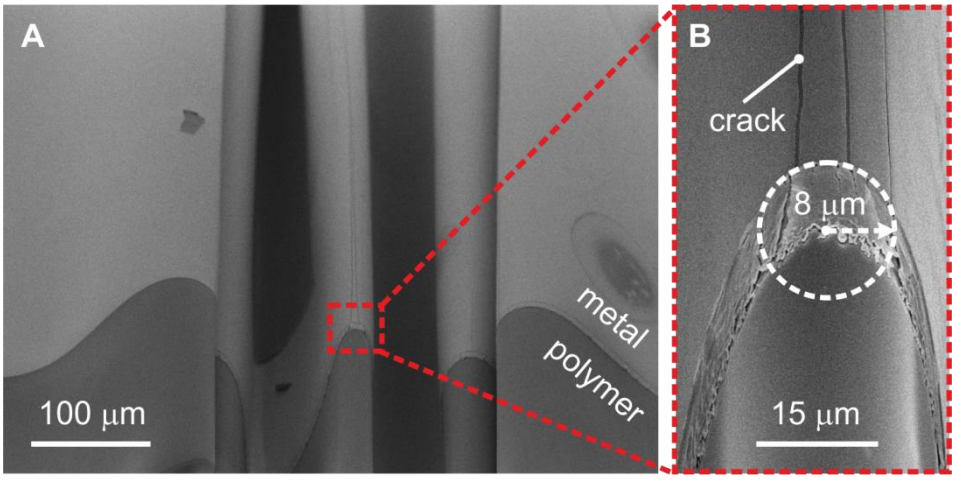

fig. S7. Development of cracks in strongly curved devices. (**A**) SEM top view image of a wrinkled spin valve sensor. The close up of the region indicated with a red frame in (A) is shown in (**B**). We find that bending radii below 10 μm occasionally induce cracking of the metal layers.

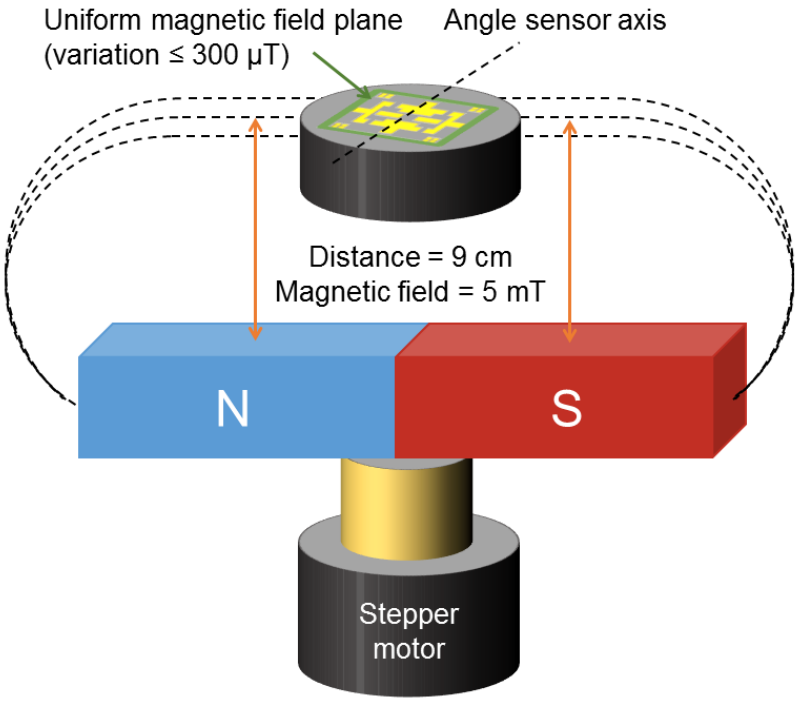

fig. S8. Schematics of the setup used to measure the angle response of the sensor in a rotating magnetic field of a permanent magnet. The setup is arranged in a way to assure minimal or no field gradient in the plane of the sensor.

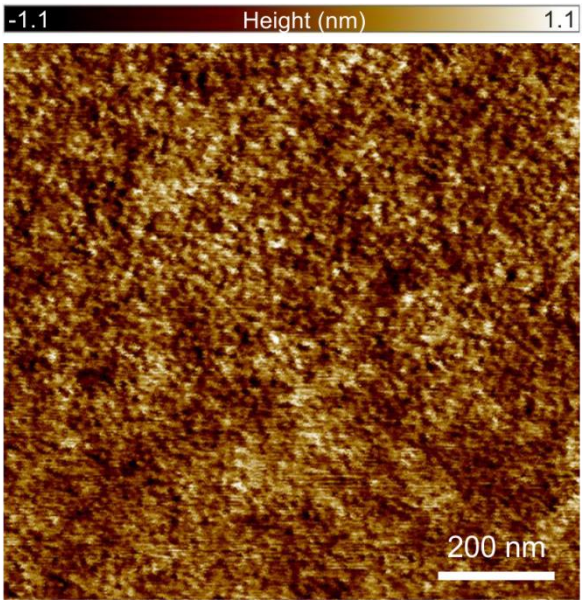

fig. S9. Surface quality characterization. Atomic force microscopy (AFM) image of the 1.7 µm thick polyimide foils. A height map of the imaged 1 x 1 μm^2 region of the foil reveals a flat surface with a root mean squared roughness of below 1 nm.

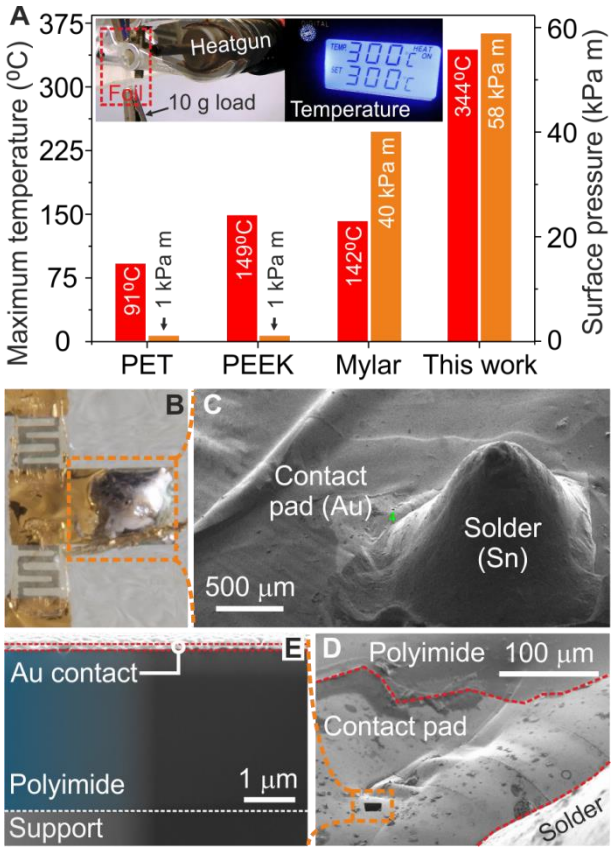

fig. S10. Thermal stability of the foils. (**A**) Maximum temperature, which the foils withstand (red-colored bars). For comparison, we used high performance commercial foils like 100 µm thick PET, 100 µm thick polyetheretherketone (PEEK) and 2.5 µm thick Dupont's Mylar. During the experiment, each of the foils is clamped at the top and a constant load of 10 g is attached to the bottom. The foils are exposed to a heat flow of a heatgun. The 1.7 µm thick polyimide foil withstands a continuous heating at 300ºC at a constant load of 10 g attached to the bottom of the foil (inset in a). The corresponding surface pressure experienced by each foil is presented with orange-colored bars. Optical microscopy image revealing one of the locations with a soldered contact (**B**) and a corresponding SEM image (**C**). (**D**) Magnified SEM image (top view) of the surface next to the solder. (**E**) SEM image of the sample cross-section taken at the location of the contact pad next to the solder.

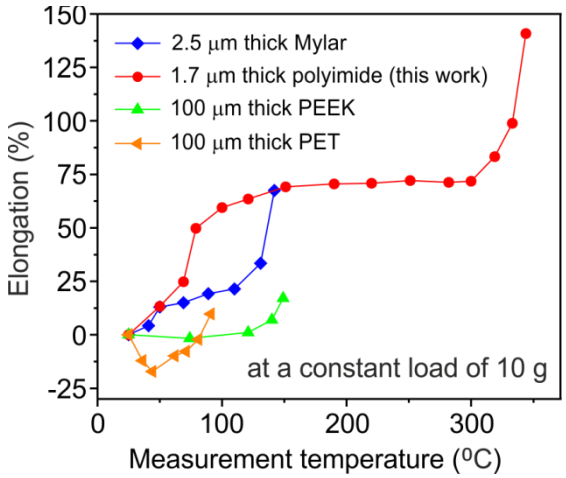

fig. S11. Elongation of polymeric foil vs. Temperature. The foils are clamped at the top and a constant load of 10 g is attached to the bottom of the foil. The evolution of the foil deformation is quantified based on the analysis of the linear separation between the clamp and the load from the Supplementary Movie S7. The novel ultrathin polyimide foil, which is 1.7 μm thick only outperforms commercial foils and carries the load up to the temperature of 344 °C. Upon increasing the temperature, two transition regions are observed for the case of the polyimide foils. The first one at 100 °C suggests a glass to rubber transition and the second one at 340 °C points towards a sudden increase in fluidity (melting) before failure.

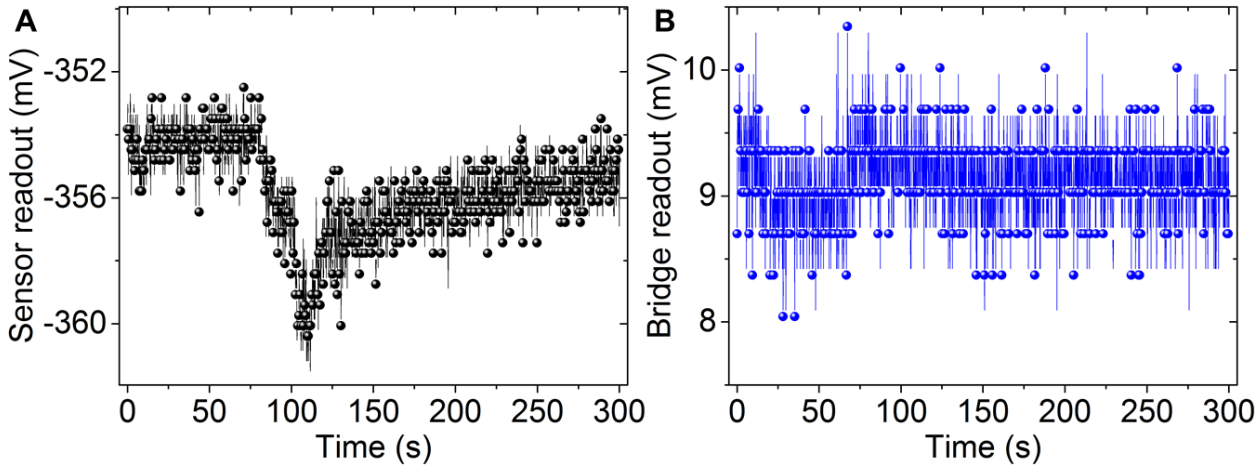

fig. S12. Temperature compensation of the sensor bridge. Time evolution of the electrical resistance of an individual spin valve sensor (**A**) and a sensor bridge (**B**) upon heating. At about 60 s, both devices are simultaneously exposed to a heat flow from a heat gun. We find that the Wheatstone bridge arrangement successfully cancels out the temperature response of the individual sensors. More details are provided in supporting movie S8.

Movie S1. Response of a spin valve upon bending. The GMR response of an individual spin valve sensor applied to a middle joint of a finger. Without an external magnetic field the sensor response is not altered by a repeated movement of the finger. The axis perpendicular (parallel) to the exchange bias direction is the low (high) sensitivity axis of the sensor.

Movie S2. Reconstruction of the magnetic field angle using 2D sensor. Upon rotation of a bar magnet, the angular response of the 2D sensor is monitored on a screen of a personal computer. The signals of the inner and outer Wheatstone bridges are displayed on a screen and the magnetic field angle is recalculated in real time. The sensor is fixed on a curved glass support suspended over the magnet such that the in-plane field magnitude is 50 Oe. For details on the setup see Fig. S4.

Movie S3. Reconstruction of the magnetic field angle under irregular field excitation. The movie demonstrates the operation of the sensor with a more "naturally" moving magnetic field source. In this case, the sensor is exposed to a magnetic field of a permanent magnet directly moved by hand. The sensor provides an unambiguous angle reconstruction independent of the tilt angle of the permanent magnet or variations of the distance between the magnetic source and the sensor.

Movie S4. Demonstrator 1: Virtual keypad applications. A 2D sensor is mounted on a wristband to provide a user with a virtual keypad which is addressed in a touchless manner by means of exposing the sensor to a magnetic field. Upon placing a small permanent magnet on a finger, the user can dial a particular combination of values on a screen which correspond to each of the input angles given by the finger.

Movie S5. Demonstrator 2: Interactive light dimming by touchless manipulation. The movie shows the manipulation of a physical property of a virtual object relying on the interaction with magnetic field exclusively. A permanent magnet defines a specific magnetic stray field pattern, which is detected by a 2D sensor applied to the palm of a hand. The change of the angular position of the sensor with respect to the static magnetic field of the magnet is measured. This signal is used to realize a touchless manipulation of the intensity of light of a virtual bulb by rotating the palm.

Movie S6. Stability of the sensor response submerged in aqueous and saline solution. The movie demonstrates a successful operation of our PDMS-encapsulated spin valve sensor operating while submerged in DI water and a sweat-like saline solution of 40 mmol/L of chloride (Fig. S5). The sensor response does not change when submerged in DI water or in salty water solution. The signal is affected only when the sensor is exposed to the magnetic field of a permanent magnet.

Movie S7. Temperature stability of the novel ultrathin polyimide foils and a commercial foil. (left) The measurement of the thermo-mechanical stability of a 1.7 µm thick polyimide foil. A 2 x 2 cm^2 piece of the foil is fixed at the top with a clamp and pulled down by a 10 g load attached at the bottom of the foil. This corresponds to the 58 kPa·m of surface pressure applied to the foil. Simultaneously a heatgun is set to progressively heat up the center of the foil. The foil can keep the load up to the temperature of 344 °C. (right) The measurement of the thermo-mechanical stability of a 2.5 µm thick Mylar foil. A 2 x 2 cm^2 piece of the foil is fixed at the top with a clamp and pulled down by a 10 g load attached at the bottom of the foil. This corresponds to the 40 kPa·m of surface pressure applied to the foil. Simultaneously a heatgun is set to progressively heat up the center of the foil. The foil can keep the load up to the temperature of 142 °C.

Movie S8. Temperature compensation of the bridge. The movie shows the time evolution of the response of a single spin valve sensor and a sensor bridge upon heating using a heat gun. A single sensor

strongly responds even to a slight temperature variation, however, no change in the readout of the bridge is observed upon the same heat treatment.